



Tuning the properties of all natural polymeric scaffolds for tendon repair with cellulose microfibers

Florencia Diaz^{a,b}, Leander Zimmermann^a, Tina P. Dale^b, Nicholas R. Forsyth^{b,c,*}, Aldo R. Boccaccini^{a,*}

^a Institute of Biomaterials, Department of Materials Science and Engineering, University of Erlangen-Nuremberg, 91058 Erlangen, Germany

^b The Guy Hilton Research Centre, School of Pharmacy and Bioengineering, Faculty of Medicine and Health Sciences, Keele University, Stoke on Trent ST4 7QB, United Kingdom

^c Vice Principals' Office, University of Aberdeen, Kings College, Aberdeen AB24 3FX, United Kingdom

ARTICLE INFO

Keywords:

Tendon tissue engineering
Biomaterials
Aligned ice templating
Polymeric scaffolds

ABSTRACT

Rotator cuff injuries affect a large percentage of the population worldwide. Surgical repair has rates of failure of up to 70%, and existing materials used in the reinforcement of injuries often lack appropriate mechanical properties and biodegradability. There is a clinical need for tendon biomaterials that enable cell attachment and proliferation, while supporting mechanically the injury site. In this work, we develop a novel all-natural polymeric scaffold for applications in the supraspinatus tendon of the shoulder. The unidirectional freezing technique is applied to a chitosan-gelatine matrix containing varying cellulose concentrations, followed by crosslinking with genipin. The viability of the technique using a custom 3D printed mould is evaluated. The scaffolds' morphology and mechanical properties are extensively characterized: the ultimate tensile strength of the material with 20% cellulose was found to increase 6-fold compared to scaffolds without cellulose; significant effects on the microstructure of the scaffold were evidenced via scanning electron microscopy. Furthermore, the biocompatibility of the materials was characterized with both porcine tendon derived cells and normal human dermal fibroblasts. All scaffolds are highly biocompatible, the incorporation of cellulose results in higher cell metabolic activity values and density of cells on the surface of the material. Scaffolds containing 20% cellulose fibers were found to possess the optimal biomechanical properties for applications in rotator cuff tendon repair.

Introduction

Tendon is a highly hierarchical tissue, mainly composed of aligned collagen type I fibers populated by tendon fibroblasts; organized into fascicles and surrounded by sheath tissues this makes up the macroscopic tendon structure (Snedeker & Foolen, 2017). Glycosaminoglycans, including decorin and biglycan, are also an important component of the extracellular matrix of tendons (James et al., 2008). The aligned morphology of these fibers gives tendons their unique mechanical properties and capacity to withstand high tensile forces (Hafeez et al., 2021).

The rotator cuff is made up of 4 muscle-tendon units, which includes the infraspinatus, supraspinatus, teres minor and subscapularis (Narayanan et al., 2018). Of the four, the supraspinatus is most often involved in tears or injuries (Itoi et al., 1995), which affect over 50% of people over the age of 60 (Rothrauff et al., 2017). Re-tears after surgical

intervention have an incidence of 38% - 46% (Carr et al., 2017), influenced by the age of the patient and the size of the initial tear (Rothrauff et al., 2017). Utilizing patch augmentation techniques has shown promise; however, the existing patch alternatives present numerous disadvantages, including inflammatory response and complications post-surgery (Chalmers & Tashjian, 2020).

Chitosan and gelatine blends have been widely studied for applications in tissue engineering (Alizadeh et al., 2013; Moshayedi et al., 2021). Gelatine is produced from the partial hydrolysis of collagen, which is the main component of the extracellular matrix of tendon (Bello et al., 2020). Collagen has raised concerns due to potential immunogenicity as well as high cost; thus, gelatine could present as an interesting, lower cost alternative, presenting good biocompatibility and degradability. Chitosan was chosen in this work as it closely mimics the glycosaminoglycans present in native tendon tissue (Muzzarelli et al., 1988). Scaffolds produced with gelatine and chitosan, though

* Corresponding authors.

E-mail addresses: nicholas.forsyth@abdn.ac.uk (N.R. Forsyth), aldo.boccaccini@ww.uni-erlangen.de (A.R. Boccaccini).

<https://doi.org/10.1016/j.carpta.2024.100447>

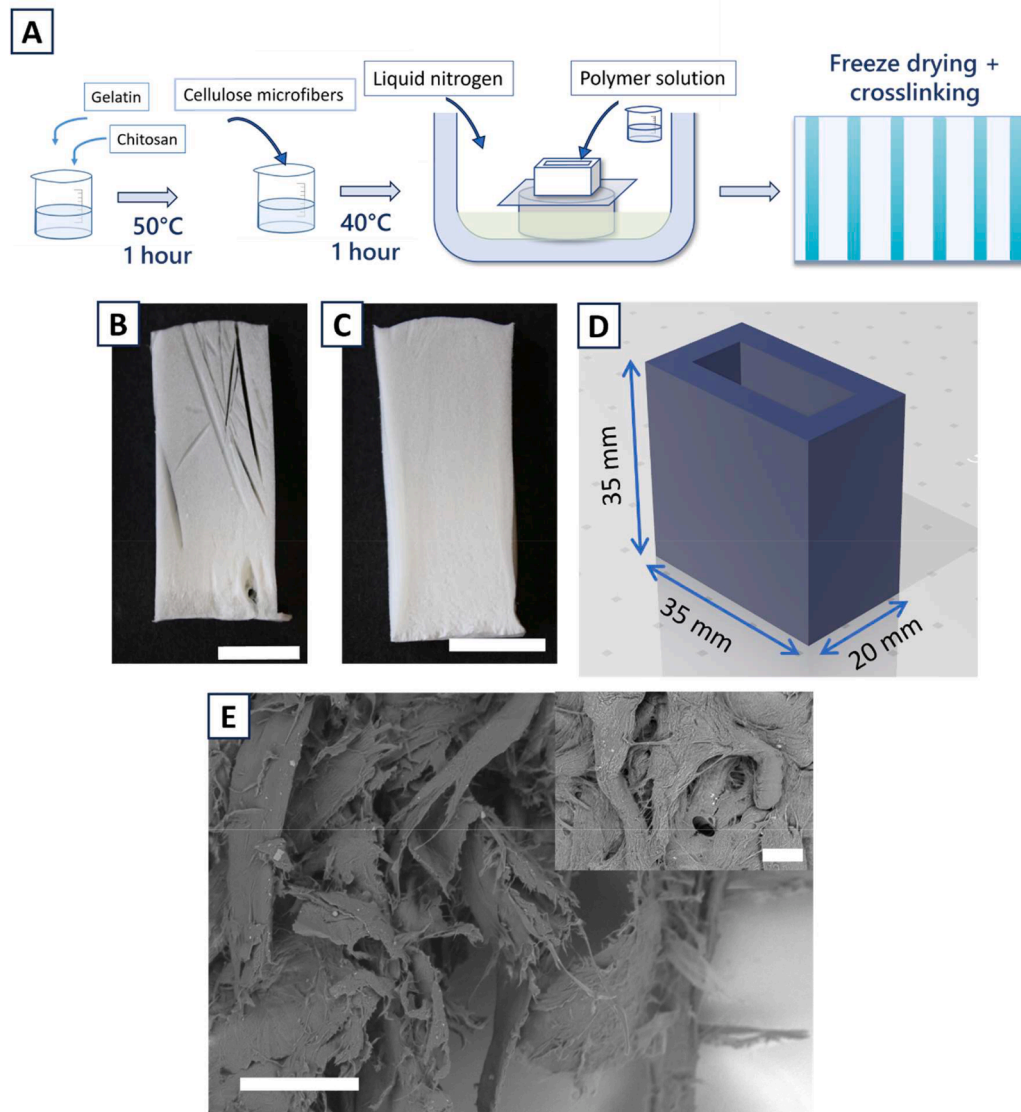


Fig. 1. Overview of the unidirectional freeze-drying process. A: Main steps involved in the fabrication of the scaffolds, including a cross-section view of the formation of aligned ice lamellae. B: Cross-section of 0% CMF pre-scaffold. C: Cross-section of 30% CMF pre-scaffold. Scale bar: 1 cm. D: View of the printed mould, including the exterior dimensions. E: SEM image of the cellulose microfibers. Scale bar large image: 50 μm . Scale bar inset image: 20 μm .

presenting many promising properties, do not possess the necessary mechanical properties for applications in rotator cuff tendon (Mao et al., 2003; Pezeshki Modaress et al., 2012). Cellulose, an abundant organic polysaccharide, has been used to modify and optimize different properties of materials (Miao & Hamad, 2013). Cellulose fibers are a popular choice due to their high stiffness and strength, which paired with their biocompatibility make them an interesting alternative for applications that require mechanical reinforcement (Campodoni et al., 2019). Though many forms of cellulose fibers have been studied, cellulose microfibers, with diameters in the range of 3 – 30 μm , have shown promise in improving the compressive strength of a sodium alginate - polyacrylamide hydrogel 3-fold (Sriraveeroj et al., 2022), and the tensile strength of a gelatine freeze-dried scaffolds 5-fold, for materials with applications in tissue engineering (Xing et al., 2010).

Furthermore, scaffolds for tendon tissue engineering should possess an aligned morphology mimicking that of the native tissue; this structure is important for the mechanical properties, cell alignment and immune response (Beldjilali-Labro et al., 2018). An aligned topography has been found to direct macrophage polarization towards an

anti-inflammatory phenotype (Hou et al., 2021), and promote the alignment and proliferation of tendon cells. (Caliari & Harley, 2011b). Significant increases in mechanical properties of anisotropic scaffolds compared with their isotropic counterparts have similarly been observed. (Zhao et al., 2021)

Ice segregation induced self-assembly is a well-known technique for producing porous scaffolds with anisotropic pore structures (Deville, 2010; Joukhdar et al., 2021; Qin et al., 2021). By placing the polymeric solution in contact with a cold surface, ice grows in a direction perpendicular to the cold plate, which after sublimation results in a material with aligned pores. (Diaz et al., 2023) This low cost, high yield technique has been previously applied for the development of scaffolds for tendon tissue engineering (Caliari & Harley, 2011b; Chen et al., 2021; Sandri et al., 2016); however, further work on the relationship between pore size, mechanical properties, and polymeric matrix is needed.

Crosslinking is the process of producing bonds between the polymeric chains, leading to the improvement of the material's properties (Tillet et al., 2011). Genipin is a non-toxic, natural crosslinker, that acts

by reacting with the primary amines present in both gelatine and chitosan (Yibin Yu et al., 2021). Genipin crosslinking has been shown to significantly improve both the degradation behaviour and the mechanical properties of polymers (Alfredo Uquillas et al., 2012; Entekhabi et al., 2020).

For studying the biocompatibility of tendon biomaterials, tendon derived stem cells have emerged as a promising alternative to the commonly used mesenchymal stem cells, in light of their good proliferative capacity and differentiation potential (Rui et al., 2010). Furthermore, evaluating the compatibility of the material with tenocytes remains essential, as they are the primary cell population in tendon (Beldjilali-Labro et al., 2018). Studies have indicated that culturing these cells in reduced oxygen concentrations, thus closer mimicking their native microenvironment (commonly referred to as physoxia), can improve their proliferative speed (Lee et al., 2012; Yang Yu et al., 2017). However, less is known about in-vitro culture of cells under physoxia in a complex 3D environment.

In this work, we have set out to investigate three main objectives: The viability of a 3D printed mould as a template for the freezing of a gelatine-chitosan scaffold; the influence of the incorporation of cellulose microfibers on a chitosan-gelatine matrix, produced by unidirectional freeze drying and crosslinked with genipin, on the structure of the scaffolds, its mechanical properties and degradation behaviour; and the attachment and proliferation of tendon derived stem cells and tenocytes cultured under two oxygen conditions.

Materials and methods

Gelatine type A, 300 g bloom, from porcine skin (suitable for cell culture grade, 70–90% protein), acetic acid (99%), ethanol (absolute) and phosphate buffered saline (PBS) powder were purchased from Sigma Aldrich. Microfibrillated cellulose (CMF) suspension, 3% w/w, with an average fiber diameter of 8 – 10 μm , was kindly provided by Weidmann Fiber Technology. Genipin ($\geq 98\%$) was purchased from Glentham Life Sciences. ChitoClear® chitosan ($\geq 99\%$) with degree of deacetylation $\geq 95\%$ and average molecular weight of 80 kDa was purchased from Primex Iceland. Calcein AM and alamarBlue were purchased from Fisher Scientific, UK. All materials were used without further modification.

Pre-scaffold preparation

Chitosan was dissolved at 2% w/v in 1% acetic acid by stirring at room temperature overnight. A 10% gelatine solution was prepared with ultrapure water, at 50 °C under constant stirring. The two solutions were mixed at a 1:1 ratio for 1 hour at 40 °C. The resulting solution was centrifuged to remove bubbles and CMFs were added to the desired ratio, ranging from 0% to 30% cellulose fibers to polymer.

The resulting solution was cast onto custom 3D printed moulds (dimensions detailed in Fig. 1) lined with aluminium foil on one side and placed onto a metallic plate in direct contact with liquid nitrogen vapor. After 1 hour, the moulds containing the frozen polymeric solution were placed in the freezer at –20 °C until ready to freeze dry, for no longer than 3 h. Finally, the frozen suspension was lyophilized for 72 h in a Christ-Alpha 2–4 LD plus freeze dryer, with an ice condenser temperature of –55 °C and pressure of 0,1 mbar. Once dry, the scaffolds easily peel away from the 3D printed moulds and can be removed and crosslinked.

Crosslinking

Pre-scaffolds were cut manually, using double sided razor blades, to dimensions approximately 5 mm x 5 mm x 1 mm for all tests, except tensile testing, for which samples were cut to approximately 30 mm x 5 mm x 1 mm. Afterwards, they were submerged in a crosslinking solution of 1% genipin in ethanol, and incubated at 37 °C. After 48 h, samples

were removed from the crosslinking solution, washed in quadruplicate with ultrapure water, and freeze dried again. All characterizations were repeated in triplicate.

Microstructure analysis

Cross-sections of the pre-scaffolds were imaged with a Canon EOS 2000D digital camera. Scaffold microstructure (after the crosslinking process) was analysed via Scanning Electron Microscopy, (Everhart–Thornley detector, AURIGA base 55, Carl Zeiss, Oberkochen, Germany), under a voltage of 3 kV. For imaging, completely dry scaffolds were manually cut to fit a 1 cm^2 metallic sample holder and attached to the holder using double sided carbon tape. Next, they were sputter coated (Q150T SputterCoater, Quorum Technologies) with gold for 50 s to prevent the effect of charging on the imaged, and they were immediately imaged. Pore width was calculated from at least 50 individual pores, with the software ImageJ. For imaging the cellulose microfibers, they were dried in an oven at 60 °C until fully dry and imaged without further modification.

Porosity

Porosity was calculated via an indirect method, as previously reported (Alizadeh et al., 2013) The samples were measured for all dimensions with a calliper to a precision of 0,01 mm in at least three different places and then averaged; and weighed with a scale of precision 0,1 mg. The volume of each sample was calculated by multiplying its average length, width and thickness. Finally, porosity was calculated according to Eq. (1):

$$\text{Porosity (\%)} = \left(1 - \frac{\rho_f}{\rho_s}\right) * 100\% \quad (1)$$

Where ρ_s is the density of the scaffolds, calculated as weight divided by volume, and ρ_f is the density of a non-porous film, produced by casting the polymeric solution into a mould and allowing it to dry for 2 days; and calculated similarly.

Wettability

Wettability was assessed with a contact angle goniometer (DSA 100, KRÜSS GmbH Co., Hamburg, Germany). A 10 μL drop of water was deposited on the surface of a sample and 10 measurements were taken. Values between the right and left side of the drop were averaged and the mean contact angle determined.

PBS swelling

Samples were weighed with a scale of precision 0,1 mg and incubated in 10 mL of PBS for 1, 8 and 24 h at 37 °C in a shaking incubator. Following incubation, they were gently patted dry to remove excess water and weighed again, after minimal manipulation to avoid the removal of absorbed liquid. Swelling ratio was calculated according to Eq. (2):

$$\% \text{ Swelling} = \frac{M_s}{M_o} * 100\% \quad (2)$$

Where M_s is the mass of the scaffold after swelling and M_o is the initial mass before immersion.

Chemical structure

Chemical structure was evaluated with Fourier Transform Infrared Spectroscopy attenuated total reflectance (FTIR-ATR). Absorbance values between 400 cm^{-1} and 4000 cm^{-1} were measured with 40 scans per sample and a resolution of 4 cm^{-1} at room temperature.

Degradation

Samples were weighed following freeze drying and incubated in 10 mL of PBS up to 45 days at 37 °C in a shaking incubator. At different time points, samples in triplicate were removed from the PBS and incubated for 1 hour in distilled water, to remove any traces of salt deposits from the PBS. They were gently patted dry and freeze dried again, following freezing overnight at -20 °C. Finally, they were weighed in the same balance.

The remaining mass was calculated according to Eq. 3:

$$\text{Remaining mass (\%)} = \frac{M_t}{M_o} * 100\%$$

Where M_t is the mass after freeze drying at time “t” after immersion and M_o is the initial mass. PBS was refreshed once a week.

Tensile testing

Scaffolds were tested in both dry and swollen conditions using samples with dimensions of 30 mm x 5 mm x 1 mm. All samples were directly fixed to the device, clamping 5 mm of the sample on each side. For dry testing, samples were tested after crosslinking and freeze-drying. For wet testing, samples were immersed in PBS for 1 hour, then removed from the solution and the excess liquid patted dry. Samples were mounted in an Instron® 5967 Universal Testing device equipped with a 100 N load cell. Measurements were carried out at a rate of 1 mm/min until breaking.

Cell culture with primary porcine tendon cells

Tenocytes (TNCs) and tendon derived stem cells (TDSCs) were extracted from pig tendon according to a previously established protocol. (Yang et al., 2018) TNCs were cultured in Dulbecco's Minimal Essential Medium with 4,5 g/L glucose content, supplemented with 10% foetal bovine serum, 1% l-glutamine, 1% non-essential amino acids and 1% Penicillin-Streptomycin. TDSCs were cultured in Dulbecco's Minimal Essential Medium with 1 g/L glucose content, supplemented with 15% foetal bovine serum, 2,5 ng/mL stem cell growth factor, 2,5 ng/mL basic fibroblast growth factor, 0,4 ng/mL epithelial growth factor and 1% Penicillin-Streptomycin. After reaching 85–90% confluency, cells were detached with trypsin and concentrated by centrifugation. Scaffolds were placed in a suspension 48 well plate and sterilized by irradiation with UV light for 1 hour followed by immersion in 70% ethanol for 30 min. They were washed in triplicate with PBS, immersed in cell culture medium and incubated at 37 °C before seeding. After 1 hour, the medium was removed, and cells were seeded on the surface with a concentration of 1×10^5 cells/cm², using a total volume of 20 µL. Samples were placed in an incubator at 37 °C overnight, after which 400 µL of fresh culture medium were added and incubated until measurement. Cell culture medium was exchanged twice a week. All experiments were carried out in an atmosphere of 5% CO₂, under oxygen concentrations of 21% and 2%, to evaluate the effects of air oxygen and physioxia on cells cultured on the 3D scaffolds.

Cell metabolic activity

After 1, 7, 14 and 21 days, cell metabolic activity was measured with the alamarBlue™ Invitrogen assay on scaffolds seeded with TDSCs and TNCs. Briefly, all the cell culture medium was removed from the samples and replaced with medium containing 10% alamarBlue™ reagent (Fisher Scientific, UK). Following incubation at 37 °C for 2 h, 80 µL aliquots were transferred to a 96 well-plate. Fluorescence was measured at Ex/Em values of 560 nm/590 nm. Fluorescence intensity values of cell seeded scaffolds were normalized against a non-seeded material control to account for the background fluorescence of the scaffolds.

Fluorescence staining

Tendon derived stem cells and tenocytes attached on the scaffold were stained after 21 days of incubation in order to investigate their morphology and their adhesion to the material. Briefly, at the intended time points, cell culture medium was removed, and scaffolds washed with PBS. Samples were incubated with a 4 µL/mL Calcein AM (Invitrogen™) in PBS solution for 1 h at 37 °C protected from light, and subsequently washed with PBS. The stained live cells were imaged with a confocal microscope (Olympus FV1200). For cross-section images, the scaffolds were fixed with a 4% paraformaldehyde solution for 1 hour following staining and washed with PBS. They were subsequently cut with a razor blade in the direction of the pores, rotated 90° and placed on a glass coverslip for imaging.

Cell culture with NHDFs

Normal Human Dermal Fibroblasts (NHDFs, PromoCell, Germany) were cultured in Dubeccos Minimal Essential Medium with 4,5 g/L glucose content, supplemented with 10% fetal bovine serum and 1% Penicillin-Streptomycin, at 37 °C, 5% CO₂ and atmospheric oxygen conditions. After reaching 90% confluency, cells were detached with 0.05% trypsin and concentrated by centrifugation. Scaffolds were disinfected similarly as when seeded with primary cells. Cells were seeded on the surface of the samples with a concentration of 1×10^4 cells/cm², using a total volume of 100 µL. Samples were placed in an incubator at 37 °C for 1 hour, after which 300 µL of fresh culture medium were added and incubated until measurement. Cell culture medium was exchanged twice a week.

Imaging of cell attachment

Following 10 days of culture with NHDFs, the cell culture medium was removed from the scaffolds, and they were immediately fixed in a 4% paraformaldehyde solution for 2 h. They were then immersed in solutions of increasing ethanol content, including 30%, 50%, 70%, 80%, 90% and 2 times 100% ethanol, for 30 min each. They were subsequently dried in a Leica EM CPD300 Critical Point Dryer. For imaging the cell layer deposited on the top of the scaffolds, the same SEM protocol was followed as detailed previously.

Statistical analysis

All data is reported as the mean ± standard deviation. Statistical difference tests were performed using one-way ANOVA, with Bonferroni post-hoc correction; except for the cell viability assay, which was analysed with two-way ANOVA and Bonferroni post-hoc correction. Three different significance levels were analysed for mean differences: $p < 0,05$ (*), $p < 0,01$ (**) and $p < 0,001$ (***)

Results

Development of freezing set-up and production of scaffolds

All scaffolds were produced from a fixed 1:1 ratio of 10% gelatine and 2% chitosan solutions; the gelatine and the chitosan are fully miscible and produce a completely homogeneous and clear solution with a yellowish colour. This ratio was chosen on the basis of preliminary experiments that analysed different ratios (not presented here), finding that increasing total polymer concentration would yield the collapse of the structure, where a lower concentration yields larger pores and a fragile structure. The main steps in the pre-scaffold preparation process are presented in Fig. 1. Different ratios of CMF to total polymer concentration were investigated, including 0%, 5%, 10%, 20% and 30% (expressed as weight of cellulose / weight of total polymer in gelatine and chitosan solution). An SEM image of an air-dried cellulose

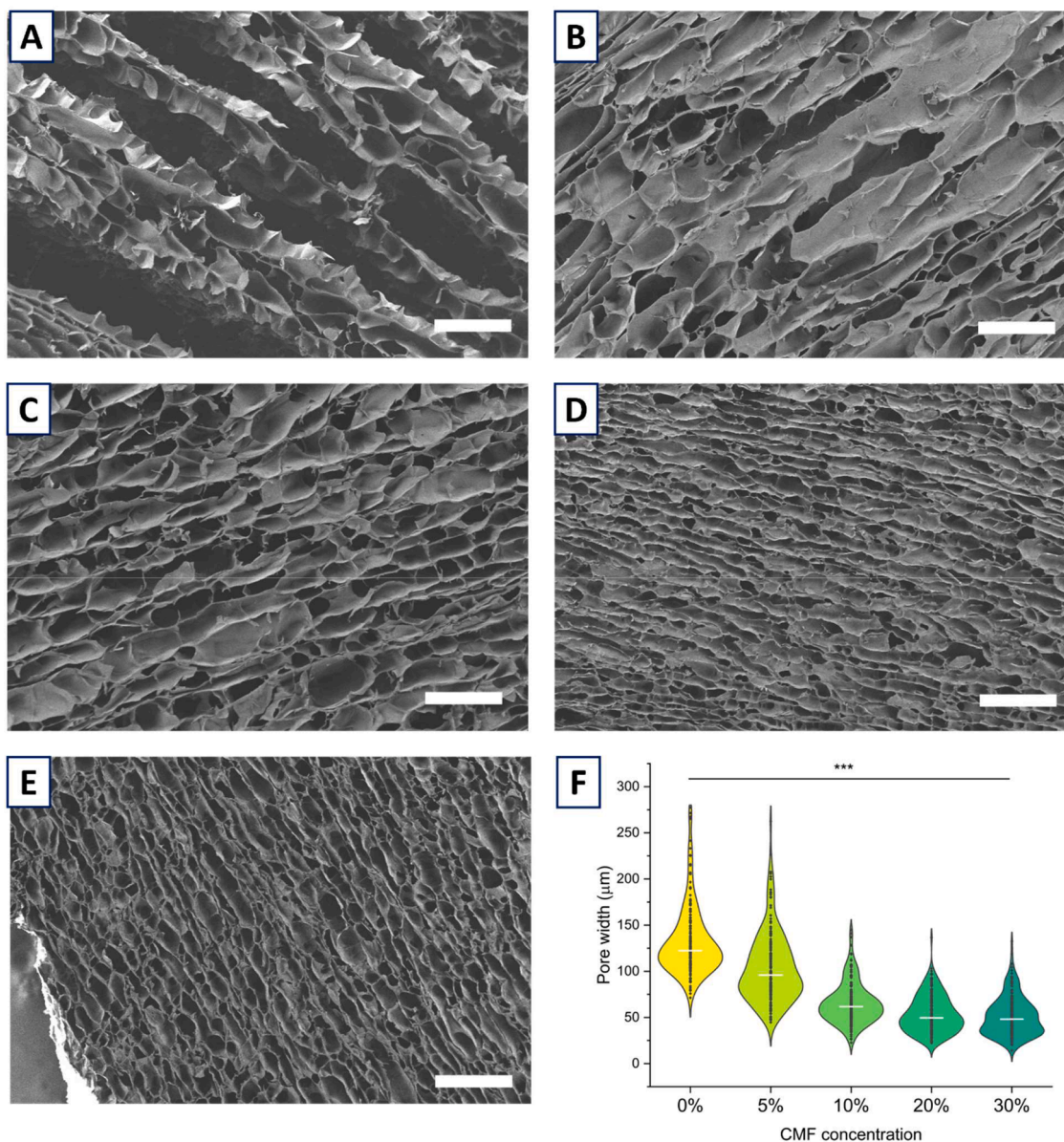


Fig. 2. SEM images of the scaffolds reveal an aligned microstructure, characteristic of the aligned ice templating technique. A decrease in pore width with increasing CMF concentration can be seen. A: 0% CMF. B: 5% CMF. C: 10% CMF. D: 20% CMF. E: 30% CMF. Scale bar: 200 µm. F: Pore width values decrease for increasing CMF concentration, where the white bar indicates the mean value. All groups exhibit a significant difference to the level of $p < 0,001$ of the mean values between each other, except the difference between the means of the 20% and 30% CMF groups ($p > 0,05$).

microfiber mat is presented in Fig. 1-E. First, we developed the set-up for conducting the unidirectional freeze-drying process in a reliable and reproducible manner. The set-up consists of a nitrogen-safe expanded polystyrene container containing an aluminium surface that contacts directly with the mould containing the polymeric solution. The mould was 3D printed with an Ultimaker S5 printer, using the synthetic polymer acrylonitrile butadiene styrene (ABS), which possesses similar thermal conductivity to the more typically used Teflon (0,18 and 0,3 W/m.K respectively), (Cai et al., 2018; Song, 2022) while aluminium has a value of 237 W/m.K. (A. Zhang & Li, 2023) The difference in conductivities between the aluminium and the mould prevents the formation of lateral ice crystals. (Nelson & Naleway, 2019) The dimensions of the mould are detailed in Fig. 1. Following the incorporation of liquid nitrogen to the bottom of the polystyrene container, ice grows vertically when the temperature of the aluminium surface gets below the freezing temperature of the polymeric solution's solvent. (Joukhdar et al., 2021) The scaffolds are subsequently freeze dried and cut to thin sections for

crosslinking. Scaffolds without cellulose present large pores and break easily with handling; whereas all scaffolds with cellulose appear more compact and are easier to handle (Fig. 1).

Cellulose concentration has a significant effect on scaffold microstructure

SEM images of the scaffolds' cross-section reveal an aligned microstructure for all CMF concentrations in the range of 0 – 30%, as shown in Fig. 2A-E. However, stark differences can be seen for the different conditions: Scaffolds without cellulose present pore walls with little to no interconnectivity that exhibit a dendritic morphology, whereas the incorporation of cellulose leads to increasing interconnectivity between the pores, that maintain a lamellar structure. Given the marked anisotropy of the pores, pore size was quantified in the perpendicular direction to the freezing (described as pore width). A significant decrease in mean pore width was found for increasing cellulose concentration with values of 138, 100, 73, 58 and 50 µm for 0% CMF, 5% CMF, 10% CMF, 20%

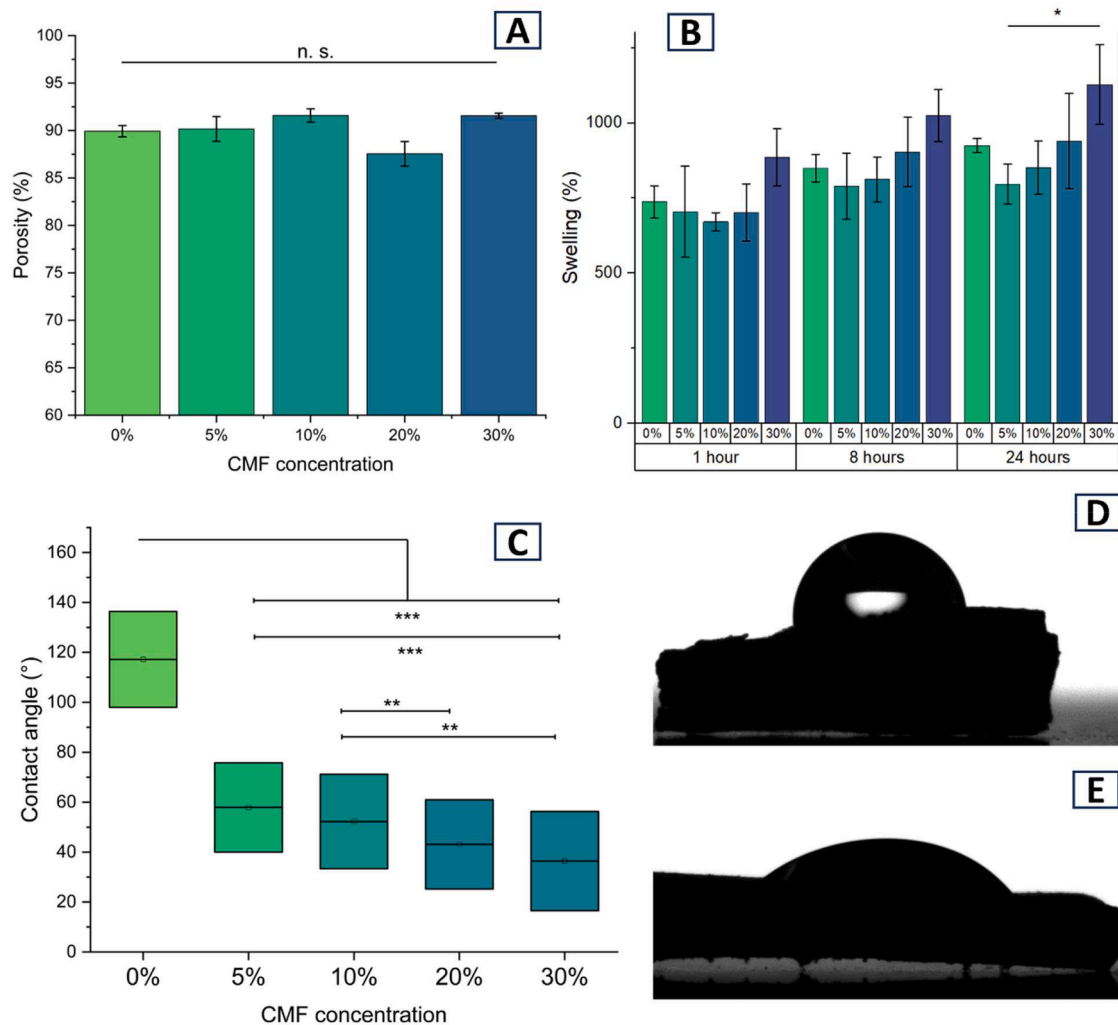


Fig. 3. Porosity and water contact properties of the scaffolds. A: Porosity values for the scaffolds. B: Swelling behaviour of scaffolds immersed in PBS. C: Contact angle of water on the surface of the biomaterials. D-E: Image of a 10 μ L water drop on the surface of the 0% CMF scaffold (D) and 30% CMF scaffold (E). Three different significance levels were analysed: $p < 0,05$ (*), $p < 0,01$ (**) and $p < 0,001$ (***).

CMF and 30% CMF respectively (Fig. 2F). The change in pore size is attributed to the entrapment of the cellulose fibers into the gelatine-chitosan matrix, resulting in the densification of the structure with a tighter pore network. The three components produce a fully homogeneous structure with no evidence of any phase separation. The molecular interactions between chitosan and gelatine are attributed to hydrogen bonds and electrostatic interactions (Qiao et al., 2017), while cellulose and gelatine are known to present electrostatic attraction at acidic pH (Leite et al., 2021).

The crystallinity of the structure has not been studied, however previous studies have found that the intrinsic crystallinity of similar cellulose microfibers is around 38% (Mbarki et al., 2019), while gelatine-chitosan composites present negligible crystallinity. (Thein-Han et al., 2009)

The determination of the optimal pore size for applications in tendon tissue engineering has to take several factors into account, and thus remains a subject of debate. The effect of pore size on equine tenocyte performance has been investigated for pore sizes in the range of 50 – 300 μ m, in an aligned porous collagen scaffold. (Caliari & Harley, 2011a; Caliari et al., 2012) These studies have indicated that pore size in a unidirectionally frozen scaffold plays a key role. Smaller pores could lead to improved initial cell attachment; however, the greater permeability of the larger pores yields enhanced proliferation in the longer term. Pore size was not found to have an effect on the capacity of cells to

align themselves with the vertical direction of the pores. Furthermore, the optimal pore morphology should allow for a sufficiently high surface area, defined as the total area available for cells to attach divided by the scaffolds total volume, for optimal cell attachment. However, this value should not be so high that it impedes cell migration into the material and nutrient diffusion.

Similarly, it's important to note that pore size will significantly impact the mechanical properties of the scaffold, as has been investigated previously, (Liu et al., 2012) where large pores could result in a largely open structure that is brittle or fragile and thus unsuitable for applications in tendon tissue.

The incorporation of cellulose affects many key properties in the scaffold

Porosity is a key property of scaffolds for tissue engineering, as pores are required for sufficient mass transfer and nutrient delivery to the cells attached on the inner pores. All scaffolds present porosity values of 85% or higher (Fig. 3-A), which indicates their suitability for this application.

Swelling behaviour of the scaffolds was measured by immersion in PBS for up to 24 h (Fig. 3-B). Understanding the liquid uptake of the material is important, as it will influence cell migration and mass transfer. Typically, increased swelling can yield better cell attachment by maximizing the available surface for the cells, however it could have a detrimental effect on the mechanical properties. (Peter et al., 2010)

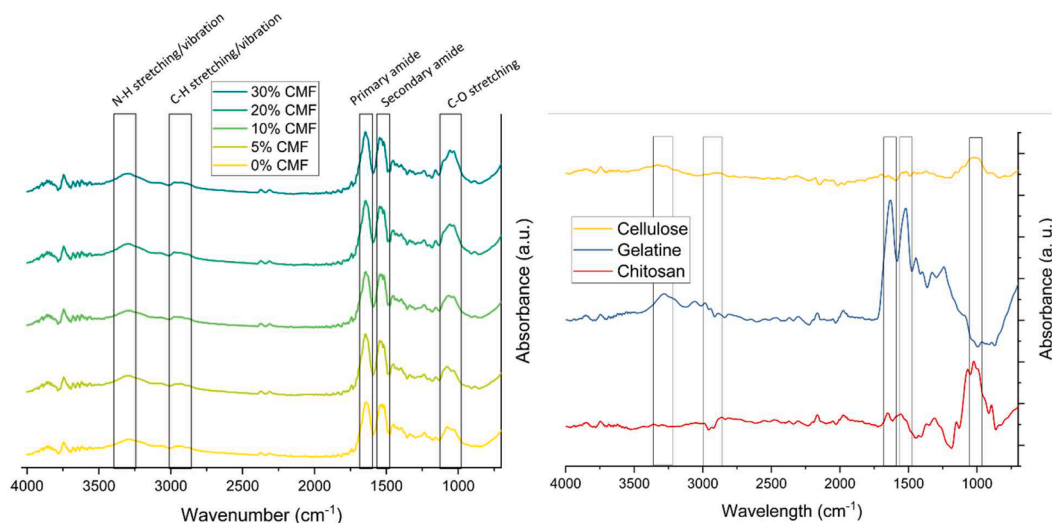


Fig. 4. FTIR analysis was used to determine the presence of cellulose on the sample. The black boxes highlight the wavenumbers that help identify main polymeric components of the scaffolds. Left: FTIR spectra of the scaffolds. Right: FTIR spectra of the unmodified polymers.

The bulk of the swelling takes place in the first hour, with gradual increases after 8 and 24 h. Increasing cellulose concentration appears to result in higher swelling behaviour after 24 h, although the 0% CMF scaffolds appear to be outliers in that trend. This could likely be due to the larger pores promoting liquid penetration and uptake. The 30% CMF scaffolds exhibit the highest swelling, possibly due to the hydrophilicity of the cellulose aiding the overall liquid uptake of the material.

Natural polymers typically exhibit predominantly hydrophilic surfaces. A gelatine film crosslinked with genipin previously presented a mean contact angle of 65° , (Tonda-Turo et al., 2011) while uncrosslinked electrospun gelatine mats presented a mean value of 75° (Y. Zhang et al., 2005). The effect of cellulose incorporation on the hydrophilicity of the material is presented in Fig. 3-C. A stark decrease in the water contact angle was found for scaffolds with 5% CMF (57°) compared to scaffolds without cellulose (116°). This value indicates that the scaffolds without CMF present a slightly hydrophobic surface, which could be due to the crosslinking in ethanol resulting in the dehydration of the surface. A further gradual decrease was found for increasing cellulose concentration, with values of 57° , 40° and 33° , for 10% CMF,

20% CMF and 30% CMF respectively. This behaviour could be attributed to the terminal hydroxyl groups present in cellulose, which can aid in the overall hydrophilicity of the material. Moderately hydrophilic surfaces have been found to be optimal for the attachment of endothelial cells and human fibroblasts, with values in the range of $35^\circ - 60^\circ$ (Arima & Iwata, 2007; Faucheux et al., 2004)

The composition of the scaffolds was verified by FTIR analysis. The spectra of the freeze dried scaffolds present contributions of the component polymers, as presented in Fig. 4. The spectra of chitosan presents a broad band in the range of $900 - 1200 \text{ cm}^{-1}$, resulting from the contributions of C—O—C bonds, C—O stretching vibrations and glycosidic bonds. Gelatine presents bands at 1633 cm^{-1} , representing the vibrations of the C—O double bonds and N—H bonds of the primary amides; and 1538 cm^{-1} , representing the stretching of the N—H bonds and vibrations of the C—N and C—C bonds of the secondary amides. (Staroszczyk et al., 2014). Similarly, gelatine exhibits a broad band in the $3400 - 3300 \text{ cm}^{-1}$ range, that can be attributed to the vibrations of the N—H of the functional groups involved in intramolecular interactions. Another broad band of lower intensity appears at $3000 -$

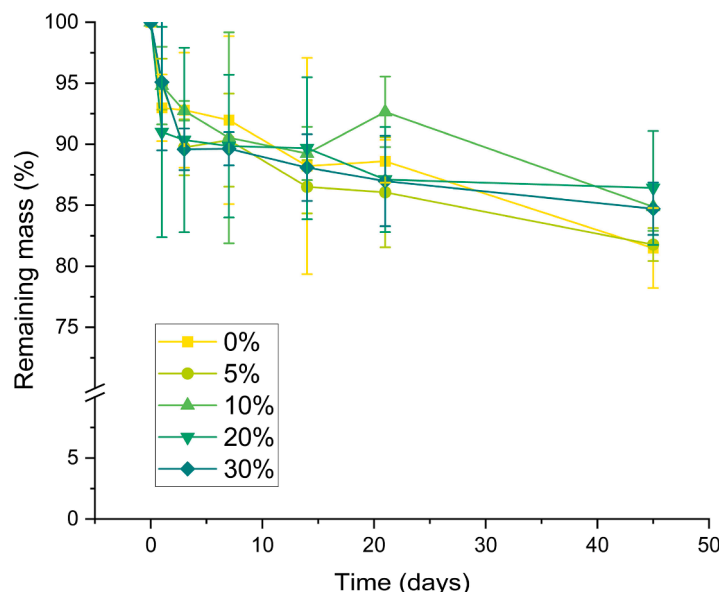


Fig. 5. Degradation profile of the scaffolds in PBS. All scaffolds degrade less than 20% in mass after 45 days, with similar behaviours across all conditions.

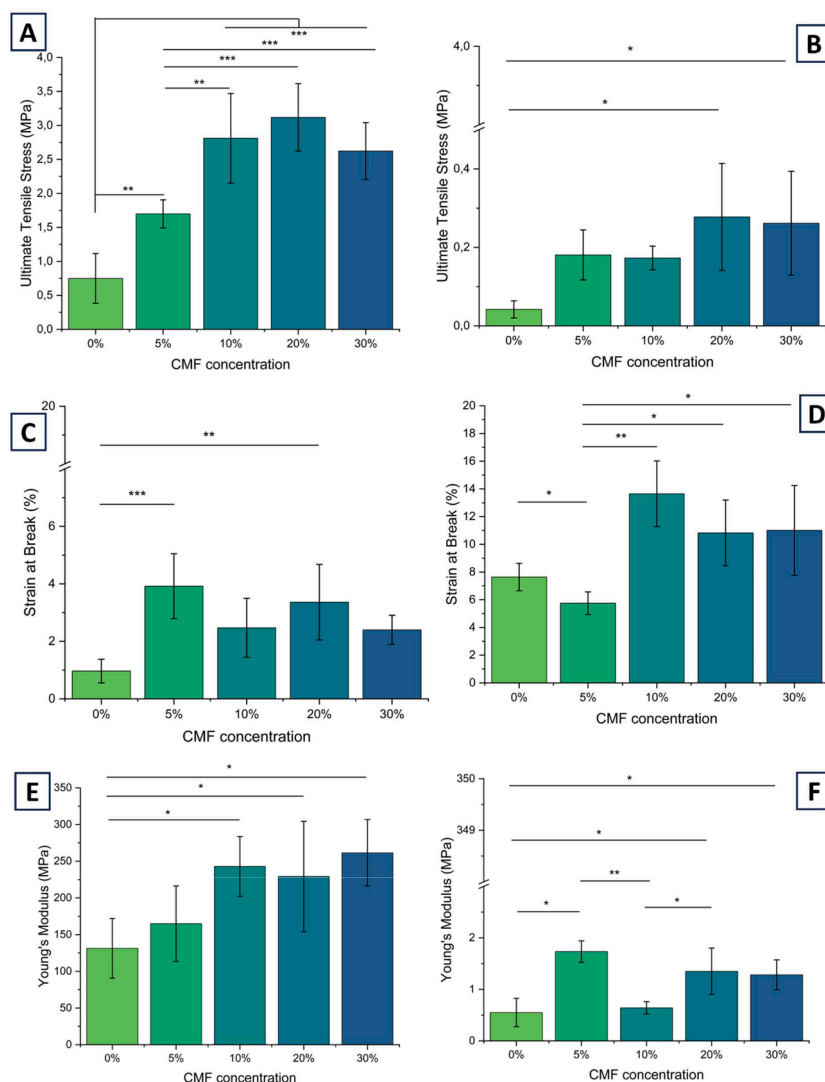


Fig. 6. Mechanical properties of dry (A, C, E) and wet (B, D, F) scaffolds. A significant increase in ultimate tensile strength and strain at break was found for scaffolds incorporating 10 – 30% CMF, compared to gelatine-chitosan scaffolds, in both dry and wet conditions. A gradual increase in elasticity modulus was found for increasing cellulose concentration for dry scaffolds; for wet scaffolds the values drop two orders of magnitude. A: Ultimate tensile strength for dry scaffolds. B: Ultimate tensile strength for wet scaffolds. C: Strain at break for dry scaffolds. D: Strain at break for wet scaffolds. E: Young's modulus for dry scaffolds. F: Young's modulus for wet scaffolds. Three different significance levels were analysed: $p < 0,05$ (*), $p < 0,01$ (**) and $p < 0,001$ (***).

2900 cm^{-1} related to the stretching and vibration of C–H bonds, and a band at 1230 cm^{-1} , corresponding to the vibrations of the C–N bond of the tertiary amide. (Nieto-Suárez et al., 2016)

All of these bands are similarly present in the scaffolds. The relative intensity of the band at 1060 cm^{-1} , with respect to the amide bands at 1633 and 1538 cm^{-1} increases gradually with the cellulose content, from 0,6 for 0% CMF scaffolds to 0,8 for 30% CMF scaffolds. This band is present for all scaffolds, as it is present in chitosan resulting from the contributions of C–O–C bonds, C–O stretching vibrations and glycosidic bonds. The increase in relative intensity is attributed to the β -1,4-glycosidic bond present in cellulose, which binds the glucose groups to produce the polysaccharide chains.

The degradation behaviour of the scaffolds is presented in Fig. 5. All conditions retain over 80% of their original mass after 45 days; experiencing the biggest loss of mass immediately after immersion in PBS where a drop of up-to 10% in mass was found for scaffolds containing 20% CMF. The CMF content does not appear to have a significant effect on the overall behaviour; rather this is hypothesized to be mainly influenced by the crosslinking conditions used. Alternative crosslinking methods will be evaluated in further work.

The tensile strength of the scaffold significantly increases with the addition of CMF

The mechanical properties of the different biomaterials were tested under uniaxial tension at a rate of 1 mm/min. A wide range of values for native human supraspinatus tendon has been reported in literature, with estimates of ultimate tensile strength (UTS) at the lower range of $4,1 \pm 1,3\text{ MPa}$ and at the higher range of $16,5 \pm 7,1\text{ MPa}$. (Chaudhury et al., 2012; Huang et al., 2005) Strain at break values have been reported between 1,11 and 4,87%. (Chaudhury et al., 2012) Whether the ideal values for the mechanical properties of a rotator cuff scaffold should match the native tendons remain a subject of debate, as it has been reported that this organ only reaches around 25 – 30% of its ultimate tensile strength during normal everyday use. (Chaudhury et al., 2012)

Strain at break, UTS and elasticity modulus were measured in both wet and dry conditions, to better understand the performance of the material in both conditions and compare them to previously reported values. As water is progressively incorporated into the polymeric network, yielding an increase in weight of over 500%, significant changes in the mechanical properties are expected. All results are

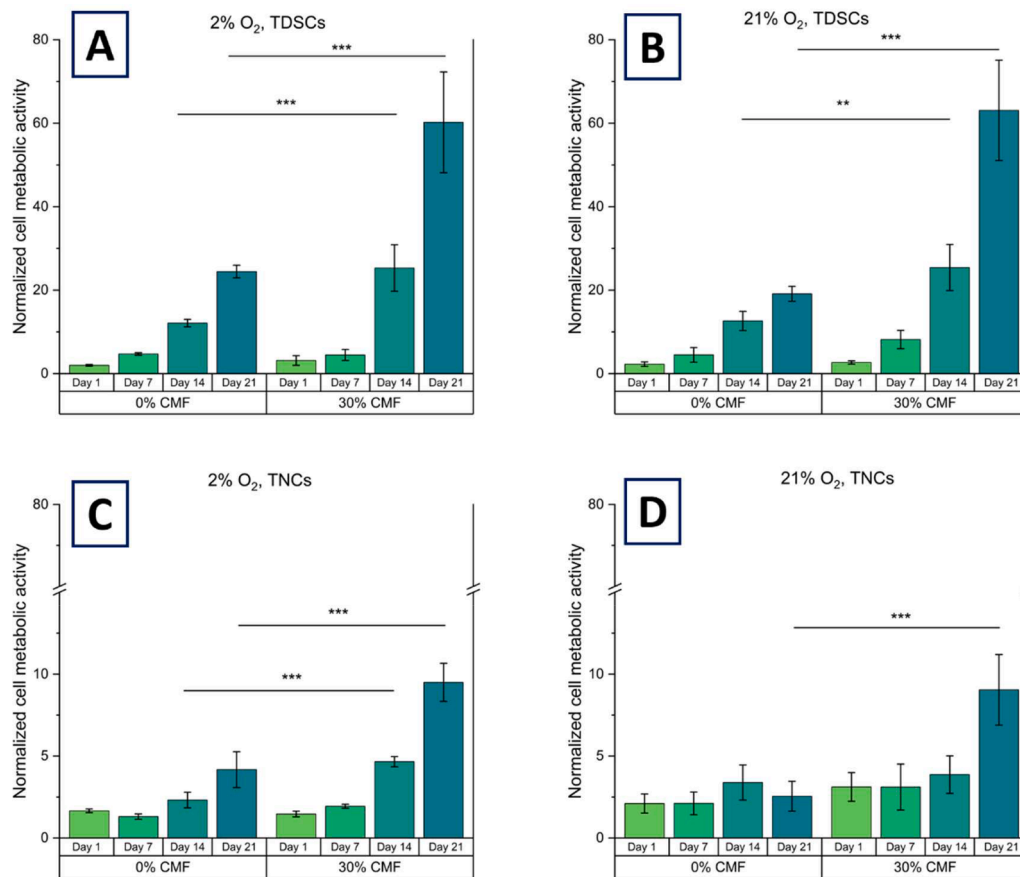


Fig. 7. Cell viability, measured with the alamar blue assay, reveals increased proliferation in 30% CMF scaffolds with respect to the 0% CMF scaffolds after 21 days. A: TDSCs cultivated in a 2% O₂ atmosphere. B: TDSCs cultivated in a 21% O₂ atmosphere. C: TNCs cultivated in a 2% O₂ atmosphere. D: TNCs cultivated in a 21% O₂ atmosphere. Results expressed as mean \pm standard deviation. Three technical replicates were analyzed. Two different significance levels were evaluated: $p < 0,01$ (**) and $p < 0,001$ (***).

presented in Fig. 6.

The ultimate tensile strength results are expressed as the highest measured stress value on the stress-strain curve. In dry conditions, all scaffolds incorporating CMF had a significantly higher UTS than without CMF. The 20% CMF scaffold presented the highest overall mean UTS value, though no significant differences were found between the 10% - 30% CMF conditions. This could be related to the pore structure of the material, as the low interconnectivity between the pore walls of the 0% CMF scaffolds yields a weak material, even after crosslinking. The progressive reduction in pore size appears to correlate with an increase in UTS for the produced scaffolds.

For wet scaffolds, the trend is similar to that of the dry, with the 20% CMF scaffolds still presenting the highest overall mean UTS values; however, the absolute UTS values are approximately one order of magnitude lower than in the dry condition.

Results for strain at break are measured as the percentual difference between the initial length of the scaffold and the length of the scaffold at the breaking point. The scaffolds without cellulose present the lowest value in dry conditions, as the large pores yield a fragile material that breaks easily; no significant differences were found between scaffolds with cellulose. All scaffolds present values within the range of supraspinatus tendon when dry. For both wet and dry scaffolds, the 10 - 30% CMF scaffolds exhibit improved strain values compared to the 0% CMF scaffolds, which could indicate that improving pore wall interconnection generally improves the materials properties.

The elasticity modulus, or Young's modulus, is a measure of the resistance of a material to elastic deformation when a force is applied; the presented values were calculated for a strain of 0,2%. Reported

values of Young's modulus for the supraspinatus tendon in humans range between 50 - 170 MPa. (Itoi et al., 1995) Scaffolds with 0% and 5% CMF fell within that range, whereas for scaffolds with cellulose content of 10% or higher, the elasticity modulus in the dry exceeded the target values, with mean values of 243 MPa, 229 MPa and 261 MPa for 10% CMF, 20% CMF and 30% CMF respectively. However, in wet condition, the values drop to the range of 0,5 - 2 MPa.

It is important to note that the mechanical properties could be significantly effected after cell culture, as has been demonstrated previously. (Camasão et al., 2019) The collagen rich extracellular matrix produced by the cells following incubation is expected to increase the stiffness of the material, meaning that the mechanical properties could significantly change in-vitro.

Cells attach and proliferate throughout the thickness of the scaffolds

Tendon derived stem cells and tenocytes, extracted from pig tendon trotter, were cultured and seeded on the surface of the scaffolds with a density of 1×10^5 cells/cm². All cells were used at passage 5, and scaffolds were incubated at both normoxia (21% O₂ atmosphere) and physoxia (2% O₂).

Tenocytes, also called tendon fibroblasts, can make up to 95% of tendon tissue. (Kannus, 2000) They are typically spindle shaped, and produce the bulk of tendon extracellular matrix, as well as participate in repair and regeneration processes. (Hess et al., 1989) Tendon derived stem cells maintain the capacity to differentiate into tenocytes as well as other cell types, and they morphology is tissue and species dependent. (Lui et al., 2014) They have been reported to be smaller and more

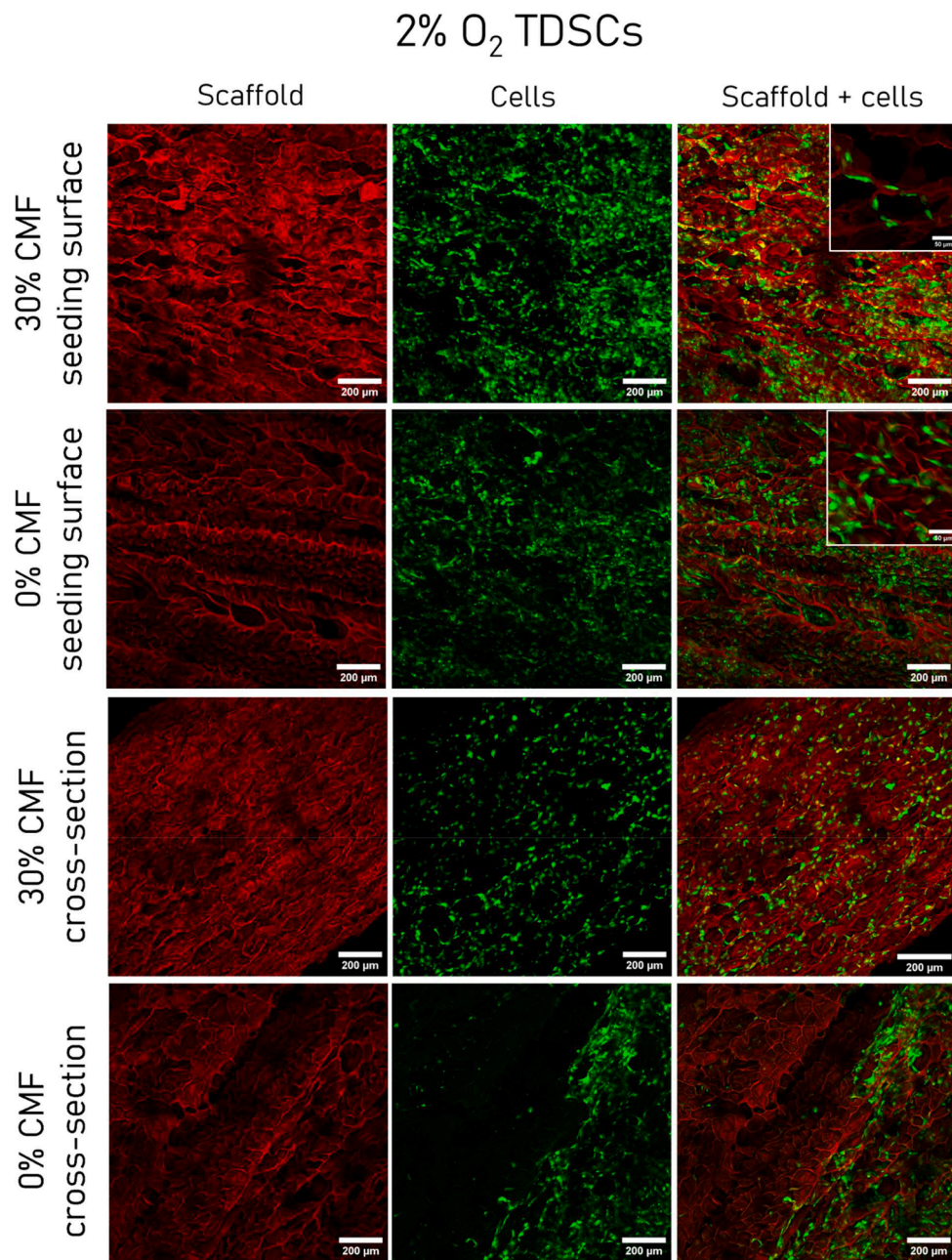


Fig. 8. Confocal microscope images of the scaffolds (in red) seeded with TDSCs stained with calcein (in green) after 21 days of incubation in 2% O₂ atmosphere exhibit large numbers of cells on both scaffolds and homogeneous distribution of cells across the surface and thickness of the scaffolds. Scale bar of large images: 200 μ m. Scale bar of inset images: 50 μ m.

rounded in shape compared to tenocytes when extracted from rabbit tendon. (Zhang & Wang, 2010)

Cell metabolic activity was measured with alamarBlue™ after 1, 7, 14, 21 days for scaffolds with 0% CMF and 30% CMF, to understand the behavior of porcine tendon derived cells on materials with distinct water contact angles and pore sizes. Results are presented in Fig. 7. Across all conditions, normalized values were found to increase in time, indicating that cells are able to grow and proliferate on the scaffolds. At days 14 and 21, a significantly ($p < 0,001$) higher value was found for the 30% CMF scaffolds compared to the 0% CMF scaffolds, across all cell types and oxygen conditions. This could be due to the increased hydrophilicity of the scaffolds with cellulose, which could allow for a greater number of cells to attach during the seeding process. The pore size, and therefore the surface-to-volume ratio of the scaffolds could also be playing an important role, as the larger pores of the 0% CMF scaffold yield a lower

total surface for the cells to attach to.

Much larger values of normalized cell viability were observed for TDSCs compared to TNCs, regardless of the time point and the oxygen concentration. TDSCs have been reported to proliferate significantly faster than TNCs when extracted from rabbit Achilles and patellar tendons, which seems to have similarly translated to the scaffold's 3D environment. (Zhang & Wang, 2010)

Furthermore, no significant differences were found in cell viability for cells cultured at different oxygen concentrations. It has been reported that human tendon stem cells cultured in 5% O₂ present faster rates of proliferation and increased stem cell gene expression compared to 20% O₂ culture. (J. Zhang & Wang, 2013) Though no such effect was found in this study, this could be due to the influence of the 3D environment, as previously reported work measured proliferation on tissue culture plastic. The age of the cells could also play a role, as it has been

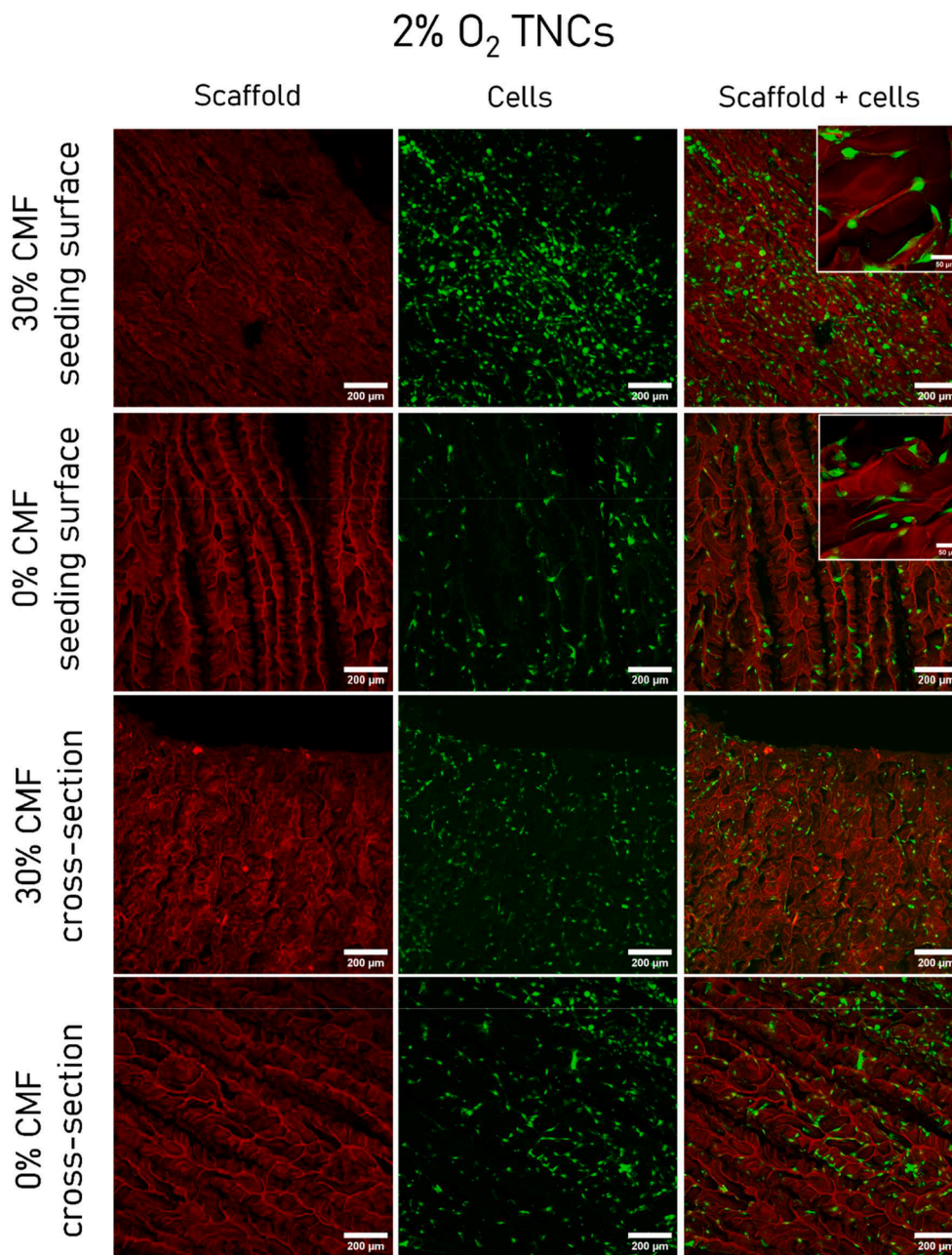


Fig. 9. Confocal microscope images of the scaffolds (in red) seeded with TNCs stained with calcein (in green) after 21 days of incubation in 2% O₂ atmosphere. Images reveal a lower cell density compared to the tendon derived stem cells, and an even distribution of cells throughout the materials. Scale bar of large images: 200 μm. Scale bar of inset images: 50 μm.

reported that typical tendon markers including scleraxis and tenascin C decrease rapidly in the first 6 passages of human tenocytes. (Mazzocca et al., 2012) However, in the case of tendon stem cells, changes in gene expression were found after much higher passage numbers. (Tan et al., 2012). Further work will evaluate the gene expression of cells cultured in the scaffolds, to better understand the effects of hypoxia on the porcine tenocytes and tendon stem cells.

Confocal images of tendon derived stem cells seeded on 0% and 30% CMF scaffolds and incubated in 2% O₂ atmosphere are presented in Fig. 8. Images include the flat surface of the scaffold that was initially seeded as well as the cross-section, with the scaffold in red (colour is due to the autofluorescence of the polymeric matrix), the live cells in green, and the resulting merged image.

A homogeneous distribution of the cells across the surface of the scaffold can be seen, with the 30% CMF scaffold appearing to present a

slightly higher cell density compared to the 0% CMF scaffold. The cells appear to have a largely elongated morphology, but no clustering or clumping could be seen on any of the samples, indicating that they are able to spread evenly throughout the surface.

For imaging the cross-section, the samples were cut and placed on their side, to better understand cell infiltration into the thickness of the material. Cells appear to be evenly distributed across the thickness of the 30% CMF scaffold, however the same was not found for the 0% CMF. Although the cells did appear to partially proliferate into the material, large sections of the cross-section were found to be void of cells. This could be due to the larger pore size impeding the migration of cells across, as well as the slight hydrophobicity of the material affecting initial cell attachment and further proliferation.

Scaffolds seeded with tenocytes at 2% oxygen were similarly stained with calcein and imaged (Fig. 9). The cell density on the seeding surface

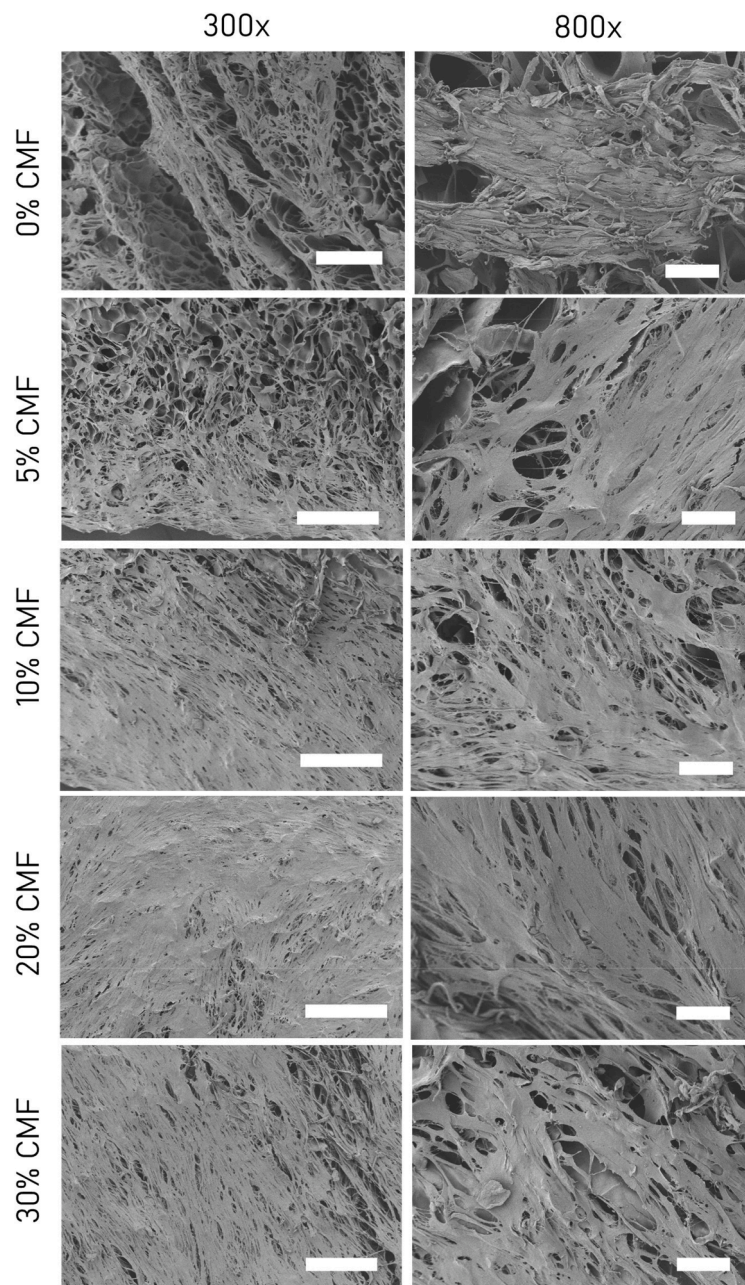


Fig. 10. SEM images of the scaffolds seeded with NHDFs after 10 days in culture reveal the formation of a layer of cells on the surface for scaffolds with 10 – 30% CMF. Scale bar of images on the left: 400 μm . Scale bar of images on the right: 50 μm .

of the 30% CMF scaffolds appears to be larger than the 0% CMF scaffolds; though for both conditions the density is lower than that of tendon derived stem cells, due to tenocytes' slower proliferation. (Clerici et al., 2023) The spindle-like morphology of the tenocytes appears preserved, as they were found to adapt to the morphology of the 3D environment. Similar behaviour was found in scaffolds seeded with both TDSCs and TNCs in 21% oxygen (not presented here).

Cells were found to be able to proliferate into the depth of the material, as shown on the cross-sections. As before, density is higher for the scaffolds with cellulose, and large areas were found in the 0% CMF without cells. For both scaffolds conditions, cells appear to largely align with the direction of the pores, as has been previously reported on anisotropic substrates. (Wu et al., 2017) It is important to note that no loss of anisotropy was found after 21 days in culture, as has been previously reported on scaffolds with a mean pore width of 292 μm , nor any significant contraction of the scaffold as a result of extended cell culture.

(Caliari et al., 2012) This could be due to the fact that the scaffolds presented in this work possess significantly improved mechanical properties, as well as smaller pores.

Although previous investigations have reported lower cell proliferation and migration values in scaffolds with pores of 100 μm or less compared to larger pores, (Caliari & Harley, 2011a) this work demonstrates that for both tendon derived stem cells and tenocytes extracted from pig, cells are capable of proliferating into the material with pores of 50 μm . Similarly, the smaller pore network is required for achieving mechanical properties in the range of tendon in dry condition.

NHDFs were seeded on the scaffolds to further understand the viability and attachment of fibroblastic cells on the surface of the material. After 10 days in culture, the seeded scaffolds were fixed, dehydrated and imaged using scanning electron microscopy (Fig. 10). The results show that for scaffolds without cellulose, the cells are not capable of forming a continuous layer on the surface, possibly due to the distance

between pore walls becoming too large for the cells to bridge. Furthermore, the cells present an irregular morphology, appearing as irregular clusters rather than smooth layers (Fig. 10, top right). On the scaffolds with 5% CMF, the cells appeared to form a smooth layer near the edges of the material, but this became discontinued toward the centre. Only for scaffolds with cellulose concentration between 10% and 30% was a continuous layer found, with cells exhibiting the typical spindle-like morphology characteristic of fibroblasts, as can be seen on the larger magnification images. Overall, the addition of cellulose to the material yields an improved adhesion and a homogenous layer of cells on the material, further reinforcing the results with the porcine tendon derived cells.

Conclusion

We have developed a novel polymeric scaffold by incorporating cellulose microfibrils into a gelatine-chitosan matrix with potential applications in tendon tissue engineering. In this work, we demonstrated the production of an anisotropic scaffold via unidirectional freezing using an inexpensive, home-made, 3D printed mould. Cellulose concentration was found to have a significant impact across key properties of the material, particularly pore size and tensile properties. The reduced pore size with increasing cellulose concentration was found to positively impact tenocytes and tendon derived stem cells' attachment and proliferation; however, for both 0% and 30% cellulose scaffolds good biocompatibility was evidenced through calcein staining and alamarBlue assay. Higher cell viability values were found for scaffolds with 30% cellulose, which could be due to its lower pore size and improved hydrophilicity. The mechanical properties achieved in this work represent a significant improvement with respect to previously published work (Caliari et al., 2012; Moncayo-Donoso et al., 2021), demonstrating that unidirectional freezing is a promising alternative for developing biomaterials suitable for applications in rotator cuff repair.

Further work will focus on the teno-inductive properties of the 20% CMF scaffold and on optimizing the crosslinking conditions with the goal of further improving the mechanical properties. Moreover the performance of the scaffold under dynamic cell culture should be characterised and the possible formation of a collagen matrix and its effects on the tensile strength of the construct must be determined.

CRedit authorship contribution statement

Florencia Diaz: Writing – original draft, Visualization, Methodology, Formal analysis, Data curation, Conceptualization. **Leander Zimmermann:** Writing – review & editing, Methodology, Data curation. **Tina P. Dale:** Writing – review & editing, Methodology, Investigation, Data curation. **Nicholas R. Forsyth:** Writing – review & editing, Supervision, Resources, Funding acquisition, Conceptualization. **Aldo R. Boccaccini:** Writing – review & editing, Supervision, Resources, Project administration, Funding acquisition, Conceptualization.

Declaration of competing interest

The authors declare that they have no known competing financial interests or personal relationships that could have appeared to influence the work reported in this paper.

Data availability

Data will be made available on request.

Acknowledgments

This paper is a part of dissemination activities of the project P4FIT. This project has received funding from the European Union's Horizon

2020 Research and Innovation Programme under the Maria Skłodowska-Curie Grant Agreement N° 955685.

References

- Alfredo Uquillas, J., Kishore, V., & Akkus, O. (2012). Genipin crosslinking elevates the strength of electrochemically aligned collagen to the level of tendons. *Journal of the Mechanical Behavior of Biomedical Materials*, 15, 176–189. <https://doi.org/10.1016/j.jmbm.2012.06.012>
- Alizadeh, M., Abbasi, F., Khoshfetrat, A. B., & Ghaleh, H. (2013). Microstructure and characteristic properties of gelatin/chitosan scaffold prepared by a combined freeze-drying/leaching method. *Materials Science & Engineering C, Materials for Biological Applications*, 33(7), 3958–3967. <https://doi.org/10.1016/j.msec.2013.05.039>
- Arima, Y., & Iwata, H. (2007). Effect of wettability and surface functional groups on protein adsorption and cell adhesion using well-defined mixed self-assembled monolayers. *Biomaterials*, 28(20), 3074–3082. <https://doi.org/10.1016/j.biomaterials.2007.03.013>
- Beldjilali-Labro, M., Garcia Garcia, A., Farhat, F., Bedoui, F., Grosset, J. F., Dufresne, M., et al. (2018). Biomaterials in Tendon and Skeletal Muscle Tissue Engineering: Current Trends and Challenges. *Materials (Basel, Switzerland)*, 11(7). <https://doi.org/10.3390/ma11071116>
- Bello, A. B., Kim, D. [Deogil], Kim, D. [Dohyun], Park, H., & Lee, S. H. (2020). Engineering and Functionalization of Gelatin Biomaterials: From Cell Culture to Medical Applications. *Tissue Engineering Part B, Reviews*, 26(2), 164–180. <https://doi.org/10.1089/ten.teb.2019.0256>
- Cai, X., Jiang, Z., Zhang, X. [Xinru], Gao, T., Yue, K., & Zhang, X. [Xinxin] (2018). Thermal property improvement of polytetrafluoroethylene nanocomposites with graphene nanoplatelets. *RSC Advances*, 8(21), 11367–11374. <https://doi.org/10.1039/C8RA01047A>
- Caliari, S. R., & Harley, B. A. C. (2011a). The effect of anisotropic collagen-GAG scaffolds and growth factor supplementation on tendon cell recruitment, alignment, and metabolic activity. *Biomaterials*, 32(23), 5330–5340. <https://doi.org/10.1016/j.biomaterials.2011.04.021>
- Caliari, S. R., & Harley, B. A. C. (2011b). The effect of anisotropic collagen-GAG scaffolds and growth factor supplementation on tendon cell recruitment, alignment, and metabolic activity. *Biomaterials*, 32(23), 5330–5340. <https://doi.org/10.1016/j.biomaterials.2011.04.021>
- Caliari, S. R., Weisgerber, D. W., Ramirez, M. A., Kelkhoff, D. O., & Harley, B. A. C. (2012). The influence of collagen-glycosaminoglycan scaffold relative density and microstructural anisotropy on tenocyte bioactivity and transcriptomic stability. *Journal of the Mechanical Behavior of Biomedical Materials*, 11, 27–40. <https://doi.org/10.1016/j.jmbm.2011.12.004>
- Camasao, D. B., Pezzoli, D., Loy, C., Kumra, H., Levesque, L., Reinhardt, D. P., et al. (2019). Increasing Cell Seeding Density Improves Elastin Expression and Mechanical Properties in Collagen Gel-Based Scaffolds Cellularized with Smooth Muscle Cells. *Biotechnology Journal*, 14(3), Article e1700768. <https://doi.org/10.1002/biot.201700768>
- Campodoni, E., Heggset, E. B., Rashad, A., Ramírez-Rodríguez, G. B., Mustafa, K., Syverud, K., et al. (2019). Polymeric 3D scaffolds for tissue regeneration: Evaluation of biopolymer nanocomposite reinforced with cellulose nanofibrils. *Materials Science & Engineering C, Materials for Biological Applications*, 94, 867–878. <https://doi.org/10.1016/j.msec.2018.10.026>
- Carr, A., Cooper, C., Campbell, M. K., Rees, J., Moser, J., Beard, D. J., et al. (2017). Effectiveness of open and arthroscopic rotator cuff repair (UKUFF): A randomised controlled trial. *The Bone & Joint Journal*, 99-B(1), 107–115. <https://doi.org/10.1302/0301-620X.99B1.BJJ-2016-0424.R1>
- Chalmers, P. N., & Tashjian, R. Z. (2020). Patch Augmentation in Rotator Cuff Repair. *Current Reviews in Musculoskeletal Medicine*, 13(5), 561–571. <https://doi.org/10.1007/s12178-020-09658-4>
- Chaudhury, S., Holland, C., Thompson, M. S., Vollrath, F., & Carr, A. J. (2012). Tensile and shear mechanical properties of rotator cuff repair patches. *Journal of Shoulder and Elbow Surgery*, 21(9), 1168–1176. <https://doi.org/10.1016/j.jse.2011.08.045>
- Chen, J., Mo, Q., Sheng, R., Zhu, A., Ling, C., Luo, Y., et al. (2021). The application of human periodontal ligament stem cells and biomimetic silk scaffold for in situ tendon regeneration. *Stem Cell Research & Therapy*, 12(1), 596. <https://doi.org/10.1186/s13287-021-02661-7>
- Clerici, M., Citro, V., Byrne, A. L., Dale, T. P., Boccaccini, A. R., Della Porta, G., et al. (2023). Endotenon-Derived Type II Tendon Stem Cells Have Enhanced Proliferative and Tenogenic Potential. *International Journal of Molecular Sciences*, (20), 24. <https://doi.org/10.3390/ijms242015107>
- Deville, S. (2010). Freeze-Casting of Porous Biomaterials: Structure, Properties and Opportunities. *Materials*, 3(3), 1913–1927. <https://doi.org/10.3390/ma3031913>
- Diaz, F., Forsyth, N., & Boccaccini, A. R. (2023). Aligned Ice Templated Biomaterial Strategies for the Musculoskeletal System. *Advanced Healthcare Materials*, 12(21), Article e2203205. <https://doi.org/10.1002/adhm.202203205>
- Entekhabi, E., Haghbin Nazarpak, M., Sedighi, M., & Kazemzadeh, A. (2020). Predicting degradation rate of genipin cross-linked gelatin scaffolds with machine learning. *Materials Science & Engineering C, Materials for Biological Applications*, 107, Article 110362. <https://doi.org/10.1016/j.msec.2019.110362>
- Faucheux, N., Schweiss, R., Lützwow, K., Werner, C., & Groth, T. (2004). Self-assembled monolayers with different terminating groups as model substrates for cell adhesion studies. *Biomaterials*, 25(14), 2721–2730. <https://doi.org/10.1016/j.biomaterials.2003.09.069>
- Hafeez, M. N., d'Avanzo, N., Russo, V., Di Marzio, L., Cilirzo, F., Paolino, D., et al. (2021). Tendon Tissue Repair in Prospective of Drug Delivery, Regenerative

- Medicines, and Innovative Bioscaffolds. *Stem Cells International*, 2021, Article 1488829. <https://doi.org/10.1155/2021/1488829>
- Hess, G. P., Cappiello, W. L., Poole, R. M., & Hunter, S. C. (1989). Prevention and treatment of overuse tendon injuries. *Sports Medicine (Auckland, N.Z.)*, 8(6), 371–384. <https://doi.org/10.2165/00007256-198908060-00005>
- Hou, J., Yang, R., Vuong, I., Li, F., Kong, J., & Mao, H. Q. (2021). Biomaterials strategies to balance inflammation and tenogenesis for tendon repair. *Acta Biomaterialia*, 130, 1–16. <https://doi.org/10.1016/j.actbio.2021.05.043>
- Huang, C. Y., Wang, V. M., Pawluk, R. J., Bucchieri, J. S., Levine, W. N., Bigliani, L. U., et al. (2005). Inhomogeneous mechanical behavior of the human supraspinatus tendon under uniaxial loading. *Journal of Orthopaedic Research: Official Publication of the Orthopaedic Research Society*, 23(4), 924–930. <https://doi.org/10.1016/j.orthres.2004.02.016>
- Itoi, E., Berglund, L. J., Grabowski, J. J., Schultz, F. M., Growney, E. S., Morrey, B. F., et al. (1995). Tensile properties of the supraspinatus tendon. *Journal of Orthopaedic Research: Official Publication of the Orthopaedic Research Society*, 13(4), 578–584. <https://doi.org/10.1002/jor.1100130413>
- James, R., Kesturu, G., Balian, G., & Chhabra, A. B. (2008). Tendon: Biology, biomechanics, repair, growth factors, and evolving treatment options. *The Journal of Hand Surgery*, 33(1), 102–112. <https://doi.org/10.1016/j.jhssa.2007.09.007>
- Joukhdar, H., Seifert, A., Jüngst, T., Groll, J., Lord, M. S., & Rnjak-Kovacina, J. (2021). Ice Templating Soft Matter: Fundamental Principles and Fabrication Approaches to Tailor Pore Structure and Morphology and Their Biomedical Applications. *Advanced Materials (Deerfield Beach, Fla.)*, 33(34), Article e2100091. <https://doi.org/10.1002/adma.202100091>
- Kannus, P. (2000). Structure of the tendon connective tissue. *Scandinavian Journal of Medicine & Science in Sports*, 10(6), 312–320. <https://doi.org/10.1034/j.1600-0838.2000.0100060312.x>
- Lee, W. Y. W., Lui, P. P. Y., & Rui, Y. F. (2012). Hypoxia-mediated efficient expansion of human tendon-derived stem cells in vitro. *Tissue Engineering Part A*, 18(5–6), 484–498. <https://doi.org/10.1089/ten.tea.2011.0130>
- Leite, L. S., Moreira, F. K., Mattoso, L. H., & Bras, J. (2021). Electrostatic interactions regulate the physical properties of gelatin-cellulose nanocrystals nanocomposite films intended for biodegradable packaging. *Food Hydrocolloids*, 113, Article 106424. <https://doi.org/10.1016/j.foodhyd.2020.106424>
- Liu, X., Rahaman, M. N., Fu, Q., & Tomsia, A. P. (2012). Porous and strong bioactive glass (13-93) scaffolds prepared by unidirectional freezing of camphene-based suspensions. *Acta Biomaterialia*, 8(1), 415–423. <https://doi.org/10.1016/j.actbio.2011.07.034>
- Lui, P. P. Y., Wong, O. T., & Lee, Y. W. (2014). Application of tendon-derived stem cell sheet for the promotion of graft healing in anterior cruciate ligament reconstruction. *The American Journal of Sports Medicine*, 42(3), 681–689. <https://doi.org/10.1177/0363546513517539>
- Mao, J. S., Zhao, L. G., Yin, Y. J., & Yao, K. de (2003). Structure and properties of bilayer chitosan-gelatin scaffolds. *Biomaterials*, 24(6), 1067–1074. [https://doi.org/10.1016/S0142-9612\(02\)00442-8](https://doi.org/10.1016/S0142-9612(02)00442-8)
- Mazzocca, A. D., Chowanec, D., McCarthy, M. B., Beitzel, K., Cote, M. P., McKinnon, W., et al. (2012). In vitro changes in human tenocyte cultures obtained from proximal biceps tendon: Multiple passages result in changes in routine cell markers. *Knee Surgery, Sports Traumatology, Arthroscopy: Official Journal of the ESSKA*, 20(9), 1666–1672. <https://doi.org/10.1007/s00167-011-1711-x>
- Mbarki, K., Boumbimba, R. M., Sayari, A., & Elleuch, B. (2019). Influence of microfibers length on PDLA/cellulose microfibers biocomposites crystallinity and properties. *Polymer Bulletin*, 76(3), 1061–1079. <https://doi.org/10.1007/s00289-018-2431-x>
- Miao, C., & Hamad, W. Y. (2013). Cellulose reinforced polymer composites and nanocomposites: A critical review. *Cellulose (London, England)*, 20(5), 2221–2262. <https://doi.org/10.1007/s10750-013-0007-3>
- Moncayo-Donoso, M., Rico-Llanos, G. A., Garzón-Alvarado, D. A., Becerra, J., Visser, R., & Fontanilla, M. R. (2021). The Effect of Pore Directionality of Collagen Scaffolds on Cell Differentiation and In Vivo Osteogenesis. *Polymers*, 13(18). <https://doi.org/10.3390/polym13183187>
- Moshayedi, S., Sarpoolaky, H., & Khavandi, A. (2021). Fabrication, swelling behavior, and water absorption kinetics of genipin-crosslinked gelatin–chitosan hydrogels. *Polymer Engineering & Science*, 61(12), 3094–3103. <https://doi.org/10.1002/pen.25821>
- Muzzarelli, R., Baldassarre, V., Conti, F., Ferrara, P., Biagini, G., Gazzanelli, G., et al. (1988). Biological activity of chitosan: Ultrastructural study. *Biomaterials*, 9(3), 247–252. [https://doi.org/10.1016/0142-9612\(88\)90092-0](https://doi.org/10.1016/0142-9612(88)90092-0)
- Narayanan, G., Nair, L. S., & Laurencin, C. T. (2018). Regenerative Engineering of the Rotator Cuff of the Shoulder. *ACS Biomaterials Science & Engineering*, 4(3), 751–786. <https://doi.org/10.1021/acsbomater.7b00631>
- Nelson, I., & Naleway, S. E. (2019). Intrinsic and extrinsic control of freeze casting. *Journal of Materials Research and Technology*, 8(2), 2372–2385. <https://doi.org/10.1016/j.jmrt.2018.11.011>
- Nieto-Suárez, M., López-Quintela, M. A., & Lazzari, M. (2016). Preparation and characterization of crosslinked chitosan/gelatin scaffolds by ice segregation induced self-assembly. *Carbohydrate Polymers*, 141, 175–183. <https://doi.org/10.1016/j.carbpol.2015.12.064>
- Peter, M., Ganesh, N., Selvamurugan, N., Nair, S. V., Furuike, T., Tamura, H., et al. (2010). Preparation and characterization of chitosan–gelatin/nanohydroxyapatite composite scaffolds for tissue engineering applications. *Carbohydrate Polymers*, 80(3), 687–694. <https://doi.org/10.1016/j.carbpol.2009.11.050>
- Pezeshki Modares, M., Mirzadeh, H., & Zandi, M. (2012). Fabrication of a porous wall and higher interconnectivity scaffold comprising gelatin/chitosan via combination of salt-leaching and lyophilization methods. *Iranian Polymer Journal*, 21(3), 191–200. <https://doi.org/10.1007/s13726-012-0019-0>
- Qiao, C., Ma, X., Zhang, J. [Jianlong], & Yao, J. (2017). Molecular interactions in gelatin/chitosan composite films. *Food Chemistry*, 235, 45–50. <https://doi.org/10.1016/j.foodchem.2017.05.045>
- Qin, K., Parisi, C., & Fernandes, F. M. (2021). Recent advances in ice templating: From biomimetic composites to cell culture scaffolds and tissue engineering. *Journal of Materials Chemistry B*, 9(4), 889–907. <https://doi.org/10.1039/d0tb02506b>
- Rothrauff, B. B., Pauyo, T., Debski, R. E., Rodosky, M. W., Tuan, R. S., & Musahl, V. (2017). The Rotator Cuff Organ: Integrating Developmental Biology, Tissue Engineering, and Surgical Considerations to Treat Chronic Massive Rotator Cuff Tears. *Tissue Engineering Part B, Reviews*, 23(4), 318–335. <https://doi.org/10.1089/ten.teb.2016.0446>
- Rui, Y. F., Lui, P. P. Y., Li, G., Fu, S. C., Lee, Y. W., & Chan, K. M. (2010). Isolation and characterization of multipotent rat tendon-derived stem cells. *Tissue Engineering Part A*, 16(5), 1549–1558. <https://doi.org/10.1089/ten.tea.2009.0529>
- Sandri, M., Filardo, G., Kon, E., Panseri, S., Montesi, M., Iafisco, M., et al. (2016). Fabrication and Pilot In Vivo Study of a Collagen-BDDGE-Elastin Core-Shell Scaffold for Tendon Regeneration. *Frontiers in Bioengineering and Biotechnology*, 4, 52. <https://doi.org/10.3389/fbioe.2016.00052>
- Snedeker, J. G., & Foolen, J. (2017). Tendon injury and repair - A perspective on the basic mechanisms of tendon disease and future clinical therapy. *Acta Biomaterialia*, 63, 18–36. <https://doi.org/10.1016/j.actbio.2017.08.032>
- Song, B. (2022). Study on Dielectric and Thermal Properties of ABS/multilayer graphene Composites. *Journal of Physics: Conference Series*, 2247(1), 12011. <https://doi.org/10.1088/1742-6596/2247/1/012011>
- Sriraveeraj, N., Amornsakchai, T., Sunintaboon, P., & Watthanaphanit, A. (2022). Synergistic Reinforcement of Cellulose Microfibers from Pineapple Leaf and Ionic Cross-Linking on the Properties of Hydrogels. *ACS Omega*, 7(29), 25321–25328. <https://doi.org/10.1021/acsomega.2c02221>
- Staroszczyk, H., Sztuka, K., Wolska, J., Wojtasz-Pająk, A., & Kotodziejska, I. (2014). Interactions of fish gelatin and chitosan in uncrosslinked and crosslinked with EDC films: Ft-IR study. *Spectrochimica Acta Part A, Molecular and Biomolecular Spectroscopy*, 117, 707–712. <https://doi.org/10.1016/j.saa.2013.09.044>
- Tan, Q., Lui, P. P. Y., & Rui, Y. F. (2012). Effect of in vitro passaging on the stem cell-related properties of tendon-derived stem cells-implications in tissue engineering. *Stem Cells and Development*, 21(5), 790–800. <https://doi.org/10.1089/scd.2011.0160>
- Thein-Han, W. W., Saikhun, J., Pholpramoo, C., Misra, R. D. K., & Kitiyanant, Y. (2009). Chitosan-gelatin scaffolds for tissue engineering: Physico-chemical properties and biological response of buffalo embryonic stem cells and transfectant of GFP-buffalo embryonic stem cells. *Acta Biomaterialia*, 5(9), 3453–3466. <https://doi.org/10.1016/j.actbio.2009.05.012>
- Tillet, G., Boutevin, B., & Ameduri, B. (2011). Chemical reactions of polymer crosslinking and post-crosslinking at room and medium temperature. *Progress in Polymer Science*, 36(2), 191–217. <https://doi.org/10.1016/j.progpolymsci.2010.08.003>
- Tonda-Turo, C., Gentile, P., Saracino, S., Chiono, V., Nandagiri, V. K., Muzio, G., et al. (2011). Comparative analysis of gelatin scaffolds crosslinked by genipin and silane coupling agent. *International Journal of Biological Macromolecules*, 49(4), 700–706. <https://doi.org/10.1016/j.ijbiomac.2011.07.002>
- Wu, Y., Wong, Y. S., & Fuh, J. Y. H. (2017). Degradation behaviors of geometric cues and mechanical properties in a 3D scaffold for tendon repair. *Journal of Biomedical Materials Research Part A*, 105(4), 1138–1149. <https://doi.org/10.1002/jbm.a.35966>
- Xing, Q., Zhao, F., Chen, S., McNamara, J., Decoster, M. A., & Lvov, Y. M. (2010). Porous biocompatible three-dimensional scaffolds of cellulose microfibril/gelatin composites for cell culture. *Acta Biomaterialia*, 6(6), 2132–2139. <https://doi.org/10.1016/j.actbio.2009.12.036>
- Yang, J., Zhao, Q., Wang, K., Ma, C., Liu, H., Liu, Y., et al. (2018). Isolation, culture and biological characteristics of multipotent porcine tendon-derived stem cells. *International Journal of Molecular Medicine*, 41(6), 3611–3619. <https://doi.org/10.3892/ijmm.2018.3545>
- Yu, Y. [Yang], Lin, L., Zhou, Y., Lu, X., Shao, X., Lin, C., et al. (2017). Effect of Hypoxia on Self-Renewal Capacity and Differentiation in Human Tendon-Derived Stem Cells. *Medical Science Monitor: International Medical Journal of Experimental and Clinical Research*, 23, 1334–1339. <https://doi.org/10.12659/MSM.903892>
- Yu, Y. [Yibin], Xu, S., Li, S., & Pan, H. (2021). Genipin-cross-linked hydrogels based on biopolymers for drug delivery: A review. *Biomaterials Science*, 9(5), 1583–1597. <https://doi.org/10.1039/d0bm01403f>
- Zhang, A. [Ailing], & Li, Y. (2023). Thermal Conductivity of Aluminum Alloys-A Review. *Materials (Basel, Switzerland)*, 16(8). <https://doi.org/10.3390/ma16082972>
- Zhang, J. [Jianying], & Wang, J. H. C. (2010). Characterization of differential properties of rabbit tendon stem cells and tenocytes. *BMC Musculoskeletal Disorders*, 11(10). <https://doi.org/10.1186/1471-2474-11-10>
- Zhang, J. [Jianying], & Wang, J. H. C. (2013). Human tendon stem cells better maintain their stemness in hypoxic culture conditions. *PLoS One*, 8(4), e61424. <https://doi.org/10.1371/journal.pone.0061424>
- Zhang, Y., Ouyang, H., Lim, C. T., Ramakrishna, S., & Huang, Z. M. (2005). Electrospinning of gelatin fibers and gelatin/PCL composite fibrous scaffolds. *Journal of Biomedical Materials Research Part B, Applied Biomaterials*, 72(1), 156–165. <https://doi.org/10.1002/jbm.b.30128>
- Zhao, Z., Moay, Z. K., Lai, H. Y., Goh, B. H. R., Chua, H. M., Setyawati, M. I., et al. (2021). Characterization of Anisotropic Human Hair Keratin Scaffolds Fabricated via Directed Ice Templating. *Macromolecular Bioscience*, 21(2), Article e2000314. <https://doi.org/10.1002/mabi.202000314>